



Sodium Multivitamin Transporter-Targeted Fluorochrome Facilitates Enhanced Metabolic Evaluation of Tumors Through Coenzyme-R Dependent Intracellular Signaling Pathways

Feredun Azari^{1,2,3}  · Gregory T. Kennedy^{1,2} · Ashley Chang^{1,2} · Bilal Nadeem^{1,2} · Patrick Bou-Samra^{1,2} · Austin Chang^{1,2} · Alix Segil^{1,2} · Elizabeth Bernstein^{2,4} · Neil T. Sullivan^{2,4} · Evgeniy Eruslanov^{2,4} · James Delikatny^{2,4} · Sunil Singhal^{1,2}

Received: 30 July 2022 / Revised: 21 November 2022 / Accepted: 23 November 2022 / Published online: 19 December 2022
© The Author(s), under exclusive licence to World Molecular Imaging Society 2022

Abstract

Background Intraoperative molecular imaging (IMI)-guided resections have been shown to improve oncologic outcomes for patients undergoing surgery for solid malignancies. The technology utilizes fluorescent tracers targeting cancer cells without the use of any ionizing radiation. However, currently available targeted IMI tracers are effective only for tumors with a highly specific receptor expression profile, and there is an unmet need for IMI tracers to label a broader range of tumor types. Here, we describe the development and testing of a novel tracer (CR)-S0456 targeted to the sodium multivitamin transporter (SMVT).

Methods Preclinical models of fibrosarcoma (HT-1080), lung (A549), breast (4T1), and renal cancers (HEK-293 T) *in vitro* and *in vivo* were used for assessment of (CR)-S0456 specific tumor labeling via sodium-mediated SMVT uptake in dipotassium phosphate or choline chloride-containing media buffer. Additionally, pharmacologic inhibition of multiple intracellular coenzyme-R obligate signaling pathways, including holocarboxylase synthetase (sulconazole nitrate), PI3K/AKT/mTOR (omipalisib), and calmodulin-dependent phosphatase (calmidazolium), were investigated to assess (CR)-S0456 uptake kinetics. Human fibrosarcoma-bearing xenografts in athymic nude mice were used for tumor and metabolic-specific labeling. Novel NIR needle confocal laser endomicroscopic (nCLE) intratumoral sampling was performed to demonstrate single-cell specific labeling by CR-S0456.

Results CR-S0456 localization *in vitro* correlated with highly proliferative cell lines (MTT) and doubling time ($p < 0.05$) with the highest microscopic fluorescence detected in aggressive human fibrosarcomas (HT-1080). Coenzyme-R-specific localization was demonstrated to be SMVT-specific after competitive inhibition of internal localization with excess administration of pantothenic acid. Inhibiting the activity of SMVT by affecting sodium ion hemostasis prevented the complete uptake of CR-S0456. *In vivo* validation demonstrated (CR)-S0456 localization to xenograft models with accurate identification of primary tumors as well as margin assessment down to 1 mm³ tumor volume. Systemic treatment of xenograft-bearing mice with a dual PI3K/mTOR inhibitor suppressed intratumoral cell signaling and (CR)-S0456 uptake via a reduction in SMVT expression. Novel analysis of *in vivo* intratumoral cytologic fluorescence using near-infrared confocal laser endomicroscopy demonstrated the absence of coenzyme-R-mediated NIR fluorescence but not fibroblast activation protein (FAP)-conjugated fluorochrome, indicating specific intracellular inhibition of coenzyme-R obligate pathways.

Conclusion These findings suggest that a SMVT-targeted NIR contrast agent can be a suitable tracer for imaging a wide range of malignancies as well as evaluating metabolic response to systemic therapies, similar to PET imaging with immune checkpoint inhibitors.

Keywords Biotin · Coenzyme-R · Molecular imaging · Metabolic labeling · Near-infrared fluorochrome · PI3K/mTOR

✉ Feredun Azari
feredun.azari@pennmedicine.upenn.edu

Extended author information available on the last page of the article

Background

Surgery remains the mainstay of therapy for most solid malignancies. However, despite curative-intent resection, an unacceptably high number of malignancies recur locally due to residual disease missed at the index operation [1]. To address this problem, IMI has been developed to improve the detection and removal of cancer cells during surgery [2]. The technology involves administering a targeted optical tracer that localizes to cancer cells and can be detected by wavelength-specific camera systems during surgery. IMI has been successful in localizing small primary lesions, identifying occult synchronous and metachronous tumors, and assessing oncologic resection margins [3]. These benefits of IMI have led to improved oncologic outcomes without compromising patient safety. However, the efficacy of IMI is predicated on identifying appropriate targeted fluorochromes for cancer cells. Given tumor heterogeneity, a significant number of patients do not benefit from the currently available receptor-targeted fluorochromes [4]. Therefore, there is a need to develop additional tracers that can target a broad array of cancer types.

One of the molecular pathways that are upregulated in many malignancies is the uptake of vitamin coenzyme-R or biotin due to its role as a coenzyme in multiple metabolic pathways, including glycolysis, oxidative phosphorylation, amino acid, and lipid metabolism (Fig. 1). Coenzyme-R-dependent carboxylases include acetyl-coenzyme A (aCoA), carboxylases 1 and 2 (ACC1, ACC2), methylcrotonoyl-CoA carboxylase 1 (MCC), propionyl-CoA-carboxylase (PCC), and pyruvate carboxylase (PC) [5–8]. These pathways are also downregulated during chemotherapeutic neoadjuvant treatments, underscoring their importance in cancer progression. These carboxylases exist in an inactive form and require activation by holo-carboxylases (HC). Holocarboxylase, in turn, is activated by the biotinylation of holocarboxylase synthetase (HLCS), which is a rate-limiting step (Fig. 1) [9]. Yoon et al., in their landmark investigation of the role of coenzyme-R in intracellular metabolism, demonstrated that holocarboxylases and byproducts of coenzyme-R mediated cellular metabolism can mitigate gene expression and histone modification, further contributing to tumorigenicity in glioblastomas (Fig. 1) [10].

Given the importance of coenzyme-R in the cellular metabolism of malignant cells, SMVT, a key transporter of coenzyme-R, has been found to be overexpressed in a broad range of cancer types (Supplementary Fig. 1) [11–13]. SMVT is a sodium ion cotransporter and requires Na ion transport via the transporter to transport biotin and pantothenic acid internally. Given the evidence of

upregulation of these metabolic pathways in cancer cells and the obligate requirement of coenzyme-R, the small molecule essential vitamin serves as a natural area to explore to label a broad range of cancers that can become a “universal” molecular agent to be used during IMI. This would serve in a similar fashion as fluorodeoxyglucose-F18-tagged metabolic evaluation of cancer cells using PET-CT imaging.

In this study, we describe the preclinical evaluation of a novel coenzyme-R conjugated NIR tracer (CR)-S0456 for the detection of metabolically active cancerous cells. First, we validated the spectrophotophysical properties of (CR)-S0456 compared to other NIR fluorochromes. We then confirmed (CR)-S0456 specificity to SMVT by evaluating its internalization after inhibiting sodium ion transporters. Additionally, we explored changes in (CR)-S0456 labeling after dual PI3K/mTOR inhibitors and novel HLCS inhibition via sulconazole nitrate. Finally, we validated our *in vitro* data in murine xenografts. Our results suggest that the biotin-targeted S0456 specifically labels highly proliferative cancers through small-molecule vitamin transporters and warrants further scrutiny in human clinical trials for IMI-guided resections.

Methods

All *in vitro* experiments were performed in triplicate to ensure reproducibility. No samples or animals were excluded from the data analysis.

TCGA and cBioPortal SMVT Expression in Primary Tumor-Derived Data Set Analysis

Messenger RNA (mRNA) expression data of SLC5A6 (SMVT) in human cell lines generated by RNA-seq analysis were downloaded from the GDC data portal (TCGA), CCLE, and cBioPortal on 1/1/2022 and sorted by primary tumor “type.” Samples with no data or no SLC5A6 expression were excluded. SLC5A6 expression was then compared to normal human tissues using the cBioPortal Integrative Analysis Platform [14].

Study Drug, Qualitative and Quantitative Spectroscopic Analysis

Fluorescent Conjugate

(CR)-S0456 is a high-affinity SMVT targeting ligand (both murine and human) linked to the NIR fluorophore S0456 (Fig. 2A) (excitation 770 nm, emission 790 nm). S0456 is also the fluorochrome that is conjugated to folate in pafolacianine, which has recently been approved by the FDA.

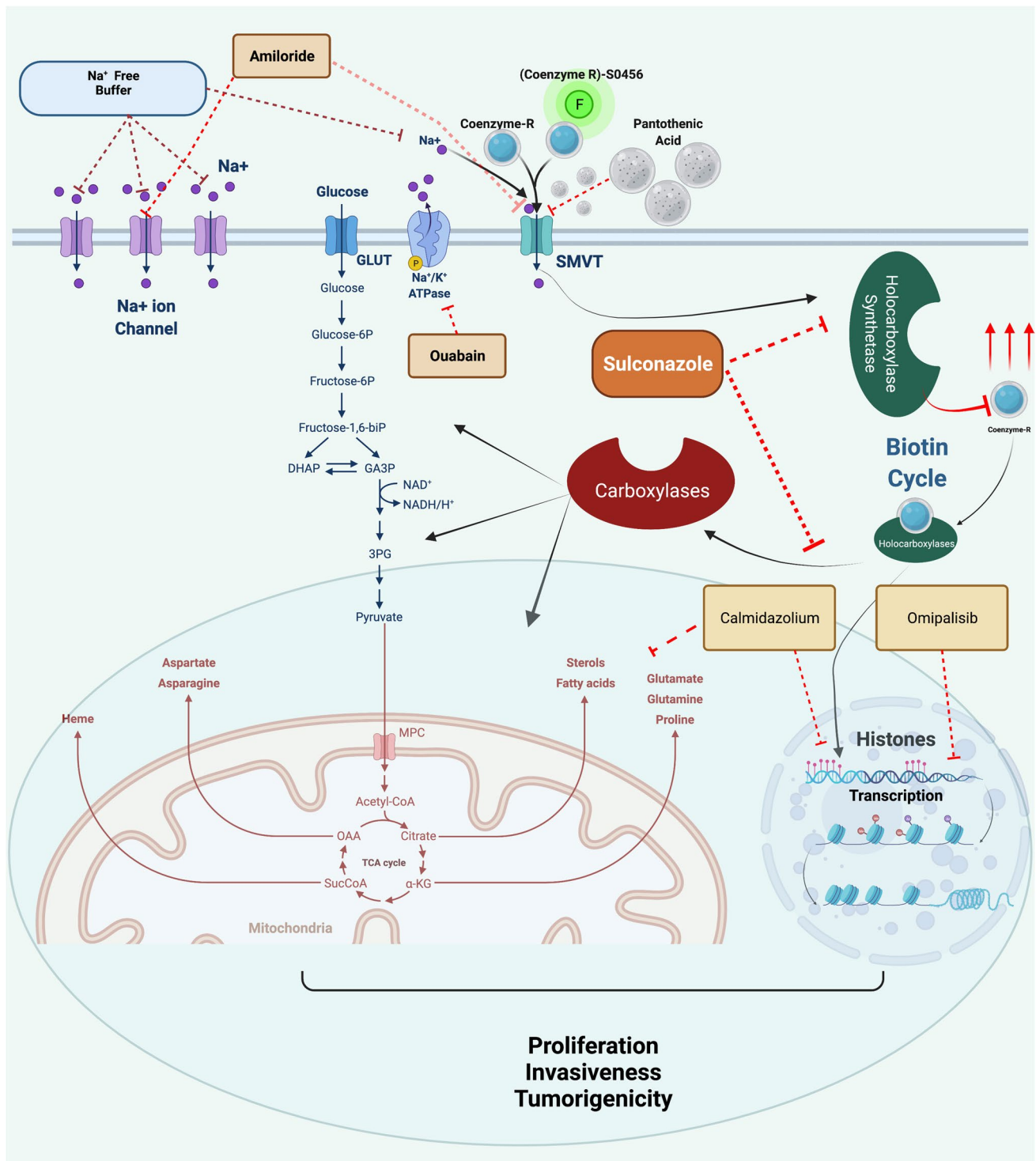


Fig. 1 Schematic demonstration of Coenzyme R-dependent enzymes. The pathways that can be exploited by conjugating coenzyme-R with the NIR fluorochrome. Coenzyme-R plays an important role in various metabolic and epigenetic functions. These pathways are upregu-

lated in aggressive cancer cells compared to normal cells. Various coenzyme-R-dependent pathways can be targeted or inhibited for intracellular delivery of vitamin-conjugated cargo.

(CR)-S0456 was synthesized and manufactured in compliance with good manufacturing practices and was stored at $-20\text{ }^{\circ}\text{C}$ in vials containing 5 mg (CR)-S0456 in 3 mL water.

Before utilization, the frozen vials were thawed, vortexed, and then diluted with 0.9% NaCl, dPBS, or culture media. The optical properties of (CR)-S0456 were analyzed after

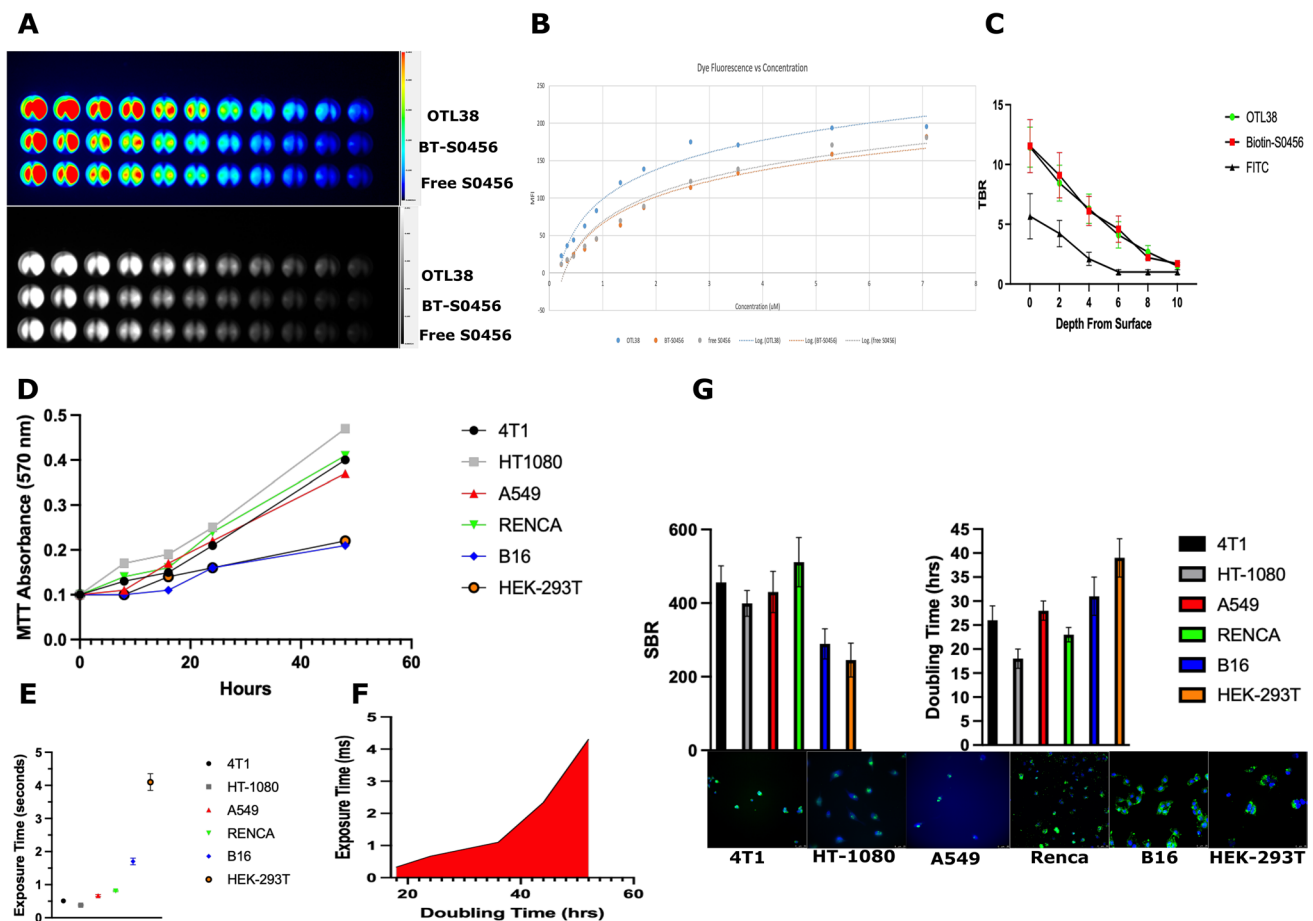


Fig. 2 **A** The microphysical properties of (CR)-S0456 demonstrate similar fluorescence parameters compared to those of pafolacianine (folate receptor alpha conjugated S0456) and **B** free nonconjugated S0456 fluorochrome. **C** Increasing the depth of penetration decreases fluorescence emission by S0456-based tracers but at a smaller rate compared to FITC. **D** Analysis of (CR)-S0456 uptake reveals fluoro-

dilution in various solvents using a UV visible/NIR spectrophotometer with a single monochromator and dual detector for the wavelength range from 190 to 2700 nm (Jasco, Oklahoma City, OK). Serial dilutions of (CR)-S0456 were performed, and the fluorescence intensity was then compared to ICG, FITC, OTL38, and free S0456 at similar dilutions.

In Vitro Studies

Cell Lines

The fibrosarcoma cell line HT-1080 (ATCC Cat# CRL-7951, RRID: CVCL_0317) was a generous gift from Dr. Steven Albelda at the University of Pennsylvania. Renca (renal cortical carcinoma), 4T1 (mammary epithelial tumor), A549 (lung carcinoma epithelial cells), B16 (melanoma), and HEK-293 T (human embryonic kidney) cell lines were obtained from the American Type Culture

chrome uptake in all viable cancer cell lines, but increased fluorescence emission is detected in **E** highly proliferative cells. HEK-293 T and B16 cells had the lowest MTT absorbance and doubling time, correlating with SBR. **E–G** Additionally, to demonstrate fluorescence emission on fluorescence microscopy, the exposure time was nearly eightfold higher in HEK-293 T cells.

Collection (ATCC, Manassas, VA). These cell lines have been described in literature reports utilizing Coenzyme-R (biotin) pathways. Cell lines were cultured in DMEM with 10% heat-inactivated FBS (Sigma–Aldrich, St. Louis, MO), 2 mM L-glutamine (Gibco, Gaithersburg, MD), 100 U/mL penicillin, and 100 µg/ml streptomycin (Gibco, Gaithersburg, MD). The cells were incubated at 37 °C in 5% CO₂ in a humidified incubator. Cells were passaged and harvested using 0.05% trypsin/EDTA solution (GIBCO). All *in vitro* experiments were performed in triplicate on separate days to ensure reproducibility. All cells were confirmed to be negative for mycoplasma contamination.

Live Cell Imaging, (CR)-S0456 Cell Uptake

Cell lines were cultured on poly-L-lysine-coated glass coverslips in 6-well plates with DMEM supplemented with 10% FBS, L-glutamine, and penicillin/streptomycin for 24 h. For

internalization time course studies, cells were treated with 10 μM (CR)-S0456 for 2 h. Coverslips were removed from the culture after varying intervals (5 min, 10 min, 30 min, 60 min, 120 min, and 180 min). To examine dose dependence, cells were incubated with different concentrations of (CR)-S0456 (1 μM , 5 μM , 10 μM , 20 μM , 50 μM , and 100 μM) for 2 h. Cells were mounted on glass slides with ProLong Gold antifade reagent with DAPI (Fisher Scientific, Waltham, MA) and imaged on a Leica DM6 B fluorescence microscope (Leica Microsystems, Wetzlar, Germany).

Cellular Uptake Studies

To assess the specific uptake of (CR)-S0456, cells were preblocked with unconjugated free coenzyme-R at 100–1000 \times the concentration of (CR)-S0456. The cells were mounted on glass slides with ProLong Gold antifade reagent with DAPI (Fisher Scientific, Waltham, MA) and imaged on a Leica DM6 B fluorescence microscope (Leica Microsystems, Wetzlar, Germany). All cellular uptake and binding studies were performed in triplicate and repeated three times.

Western Blot Analysis for Cell-Line SMVT Expression

Cells were harvested and lysed for Western blot analysis. Sodium dodecyl sulfate (SDS)-polyacrylamide gel electrophoresis and blocking were performed. The membranes were incubated with antibodies to detect SMVT (Santa Cruz Biotechnology, sc-514319) expression and glyceraldehyde-3-phosphate dehydrogenase (GAPDH). Signals were visualized with an Amersham Imager 680 (GE Life Sciences).

SMVT Sodium Ion-Dependent Uptake of (CR)-S0456

To investigate the effect of sodium dependence on SMVT-mediated (CR)-S0456 uptake, cells were cultured in a sodium-free buffer. Additionally, cells were either preincubated with ouabain (Na^+/K^+ ATPase inhibitor) or amiloride (Na^+ ion transporter inhibitor) to confirm the ion-dependent uptake of (CR)-S0456. Sodium-free buffers were used to confirm the Na^+ presence requirement for (CR)-S0456 uptake by replacing 0.9% NaCl (0.15 mol/L) or DPBS with equimolar concentrations of dipotassium phosphate or choline chloride. Cells were treated with 10 μM (CR)-S0456 for 2 h. Coverslips were removed from the culture, mounted on glass slides with ProLong Gold antifade reagent with DAPI (Fisher Scientific, Waltham, MA), and imaged on a Leica DM6 B fluorescence microscope (Leica Microsystems, Wetzlar, Germany).

Metabolic Energy Correlation with (CR)-S0456 Uptake

To investigate whether (CR)-S0456 uptake is predicated on the metabolic activity of proliferative cell lines, cells were incubated with either omipalisib (dual PI3K/mTOR inhibitor) (obtained in collaboration with Phillip Low at Purdue University) and sulconazole nitrate (Selleckchem), which has been demonstrated to be an HLCS inhibitor as detailed by Yoon et al., or calmidazolium chloride (ABCAM-AB120658). Cells were treated with 10 μM (CR)-S0456 for 2 h. Coverslips were removed from the culture, mounted on glass slides with ProLong Gold antifade reagent with DAPI (Fisher Scientific, Waltham, MA), and imaged on a Leica DM6 B fluorescence microscope (Leica Microsystems, Wetzlar, Germany).

Murine Studies

Animal studies were performed according to protocols approved by the University of Pennsylvania Institutional Animal Care and Use Committee (IACUC) in accordance with the National Institutes of Health guidelines. Female 6- to 8-week-old athymic nude mice (RRID: RGD_5508395) were purchased from Charles River and maintained on normal rodent chow. Mice were housed in a sterile environment on a standard 12-h light and dark cycle for the duration of the study. For the injection, cell lines were cultured in DMEM with 10% heat-inactivated FBS (Sigma-Aldrich, St. Louis, MO), 2 mM L-glutamine (Gibco, Gaithersburg, MD), 100 U/mL penicillin, and 100 $\mu\text{g}/\text{ml}$ streptomycin (Gibco, Gaithersburg, MD). Cells were incubated at 37 $^\circ\text{C}$ with 5% CO_2 in a humidified incubator. Cells were passaged and harvested using 0.05% trypsin/EDTA solution (GIBCO). All experiments were performed in triplicate on separate days to ensure reproducibility. All cells were confirmed to be negative for mycoplasma contamination as assessed by MycoAlert Mycoplasma Detection Kit (Lonza). Mice were subcutaneously inoculated in the flank with 1 million cells in neutral Dulbecco's PBS solution (without calcium or magnesium). Mice were monitored for tumor size and used for imaging and biodistribution. Once the tumors reached the appropriate minimum volume threshold, NIRF images were obtained on the LI-COR Pearl Impulse Imager using an excitation wavelength of 785 nm and a detection wavelength of 800 nm. Mice were sacrificed at various time points, and whole-body images were obtained. Following this, organs of interest were harvested and imaged ex vivo on a Petri dish. Data were displayed and analyzed using LI-COR Pearl Impulse Software, and the fluorescence intensity was corrected for the background signal and normalized to the surrounding tissue.

Pharmacokinetic and Biodistribution Studies

Athymic nude mice were subcutaneously inoculated in the flank with 1 million cells. Mice were monitored for tumor size and used for imaging and biodistribution when the size of the tumors reached at least $500 \pm 50 \text{ mm}^3$ for the flank xenografts. Tumor volume was periodically calculated using the formula ($3.14 \times \text{long-axis} \times \text{short-axis}^2$). Once the tumors reached the appropriate minimum volume threshold (pending cell line used), xenograft-bearing mice were injected with (CR)-S0456 at different concentrations (0–20 nM) ($n=5$ per dosing level). NIRF images were obtained on the LI-COR Pearl Impulse Imager using an excitation wavelength of 785 nm and a detection wavelength of 800 nm. Mice were sacrificed at various time points, and whole-body images were obtained. Following this, organs of interest were harvested and imaged *ex vivo*. Data were displayed and analyzed using LI-COR Pearl Impulse Software, and the fluorescence intensity was corrected for the background signal and normalized to the surrounding tissue.

Evaluation of *In Vivo* Sarcoma Labeling by (CR)-S0456 in Murine Models

After determining the optimized dosing and timing parameters, female athymic nude mice bearing flank xenografts ($n=5$ per cell line) with a tumor volume of at least $500 \pm 50 \text{ mm}^3$ were intravenously administered (CR)-S0456 (5 mg/kg, not to exceed 300 μL in tail vein injections). Twenty-four hours after (CR)-S0456 injection, mice were euthanized and imaged with the Iridium Imaging System (Vision Sense, New York, NY). Tumors were removed and imaged with the Odyssey Imaging System (LI-COR Biosciences, Lincoln, NE). Tissue sections were further analyzed by hematoxylin and eosin staining, immunohistochemistry staining for SMVT, and fluorescence microscopy (Leica Microsystems, Wetzlar, Germany). Margin assessments were analyzed by blinded observers not involved in the development of the conjugate. Randomization was not performed given the initial proof of principal studies performed in this analysis.

NIR Needle Confocal Laser Endomicroscopic Intratumoral Cytologic Evaluation

The needle probe used in the experiments contains 10,000 optical fiber bundles with an imaging depth of 55 μm , a lateral resolution of 3.5 μm , and a field of view of 325 μm .

The probe was used in conjunction with a commercially available CLE system (CellVizio, Mauna Kea Technologies, Paris, France) that generates an excitation light with a 785 nm laser that is expanded by a beam expander and reflected by a dichroic mirror. Subsequently, a two-dimensional scanning system scans the beam in the

two-dimensional plane. After scanning, the beam is relayed into the back aperture of the objective lens, which couples the excitation light into the proximal end of the optical fiber bundle in the NIR-nCLE probe. Finally, the beam is focused on the sample by a near-infrared miniature objective (at the imaging depth), which also collects the emitted fluorescence from the sample. The fluorescence at longer wavelengths is transmitted along the same path and passed through the dichroic mirror and a bandpass filter (800 to 890 nm). After passing the bandpass filter, the fluorescence is focused by a lens to pass through a pinhole that is placed at the focus of the condenser. The pinhole is used to reject the out-of-focus light. Finally, a photodiode is used to acquire optical signals and convert them into electrical signals. With the XY scanners, the imaging speed can reach 8 to 12 frames per second, which makes imaging in real-time possible. Each frame consists of 320×322 pixels. The probe is inserted into the xenograft, which detects fluorescence emission targeted to the S0456 fluorochrome wavelength.

Statistical Analysis

Data are presented as the mean \pm SEM or \pm SD as indicated. Statistical differences between the 2 groups were assessed using *t*-tests with GraphPad Prism software (GraphPad Prism, RRID:SCR_002798) and SPSS version 27 (IBM Technologies) (SPSS, RRID:SCR_002865).

One-way ANOVA followed by post hoc Tukey's test was used to analyze differences between more than two groups. Fluorescence parameter analysis was performed by ImageJ (National Institutes of Health) (ImageJ, RRID:SCR_003070) and MATLAB image segmentation analysis (MathWorks) (MATLAB, RRID:SCR_001622). Preliminary power analysis demonstrated a minimum of 5 mice per group to achieve $p < 0.05$ via one-way ANOVA. $P < 0.05$ was considered a statistically significant difference.

Results

(Coenzyme R)-S0456 Localizes to Highly Proliferative Cells

We initially compared the spectrophysical properties of (CR)-S0456 to other established NIR fluorochromes. NIR imaging of (CR)-S0456 demonstrated an MFI of 185 absorbance units [A.U.] (± 31) vs 211 A.U. (± 19) for FDA-approved agent pafolacianine ($p=0.11$). There was no difference in MFI when compared to the unconjugated fluorochrome (free S0456, same fluorochrome utilized in pafolacianine) 181 (± 21) ($p=0.23$). There was a log-linear concentration increase in fluorescence with increasing concentrations of all tracers. (CR)-S0456 demonstrated a linear

decrease in the signal-to-background ratio (SBR) associated with increasing depth from the surface (SBR 12.67 at 0 mm vs 5 at 6 mm vs 1 at 10 mm, $p < 0.01$) (Supplementary Fig. 2). (CR)-S0456 demonstrated a 2.31-fold increase in emission intensity compared to lower wavelength tracers (i.e., FITC)⁴ ($p < 0.01$) (Fig. 2A–C).

Concordant with literature reports, we wanted to explore whether (CR)-S0456 uptake would correlate with the proliferative potential of cellular organisms. The MTT assay demonstrated that the HT1080 cell line had the highest OD at 0.48 at 48 h, and the HEK-293 T and B16 cell lines had the highest OD at 0.2 at 48 h. A549, RENCA, and 4T1 cells were not significantly different at all time points prior to 48-h measurements from HT-1080 cells ($p = 0.07$) (Fig. 2D). All cell lines demonstrated uptake of (CR)-S0456 by NIR immunofluorescence microscopy (NIRF). However, to detect fluorescence, B16 (literature negative) and HEK-293 T (literature negative) cells had significantly longer exposure times (HEK-293 4.11 s, B16 1.8 s) than HT-1080 cells (0.48 s) ($p < 0.001$) (Fig. 2E, F). Furthermore, when looking at mean emission fluorescence intensity, B16 and HEK-293 T cells had the lowest SBR 237 vs other cells (398, $p < 0.05$) (Fig. 2G). Fluorescence intensity was inversely correlated with doubling and exposure time (Fig. 2F). In summary, (CR)-S0456 fluorescence correlates with the proliferative potential of the cell.

(Coenzyme R)-S0456 Requires Na⁺ Ion Co-Transport and Correlates Cell Metabolic Activity

Given that coenzyme-R uptake is mediated by SMVT, which is a sodium ion cotransporter and requires Na⁺ ion transport via the transporter to transport coenzyme-R and pantothenic acid internally (Fig. 1), we examined the inhibition of sodium ion homeostasis and the effects of coenzyme-R uptake. We examined removing Na⁺ ions completely from the media, blocking Na⁺ channels with the Na⁺ ion channel inhibitor amiloride, and Na/K ATPase inhibitors affecting (CR)-S0456 cellular internalization. Furthermore, after exploring SMVT-specific cotransport of (CR)-S0456, we explored whether inhibition of various intracellular pathways of proliferation, including coenzyme-R obligate rate-limiting steps, will affect (CR)-S0456 fluorescence uptake and emission intensity. An overview of the points of inhibition and rationale is given in Fig. 1.

Na⁺ is Critical for (CR)-S0456 Uptake via the Na⁺/SMVT Cotransporter

HT1080 cells grown in standard DMEM and isotonic saline media demonstrated similar MFIs (318 ± 37 vs 344 ± 29 , $p = 0.17$) (Fig. 3A). When the sodium ions were removed from the buffer and supplemented with either choline

chloride or dipotassium phosphate (Dibasic), there was a significant decrease ($2.89\times$) in (CR)-S0456 MFI in HT1080 cells ($p < 0.05$) with MFIs of 89 ± 6 (choline chloride) and 103 ± 11 (dipotassium phosphate) ($p < 0.05$) (Fig. 3A). Once the buffer solution was replaced with isotonic or normal growth buffer, HT1080 cells demonstrated (CR)-S0456 uptake with an MFI of 279 ± 39 . To further confirm the dependence of (CR)-S0456 on sodium ion cotransport, HT-1080 cells were treated with amiloride hydrochloride, a selective sodium transport inhibitor (Fig. 3B). The presence of amiloride demonstrated minimally (CR)-S0456 uptake into the cells, with an MFI of 91 ± 13 , which was significantly lower than that of standard media (311 ± 27 , $p < 0.05$) (Fig. 3B, E). Additionally, ouabain (Na/K ATPase inhibitor) administration in standard physiological Na⁺-containing media significantly decreased (CR)-S0456 in HT-1080 cells compared to the control (318 ± 37 vs 178 ± 26 , $p < 0.05$) in viable cells. In summary, the presence of sodium ions is critical for the cotransport of (CR)-S0456 through SMVT, in keeping with physiological coenzyme-R absorption mechanisms.

We further explored the specificity of (CR)-S0456 to SMVT receptors by preblocking HT-1080 cells with 100–1000 \times pantothenic acid (SMVT-utilizing vitamin) or folate (non-SMVT utilizing vitamin). Pantothenic acid and coenzyme-R are two small molecular vitamins that are specifically transported intracellularly via SMVT under physiological conditions. Increasing the concentration of pantothenic acid competitively inhibited (CR)-S0456 cellular uptake similar to competitive inhibition with free unconjugated coenzyme-R (Fig. 3D, E, Supplementary Figs. 3 and 4), demonstrating that (CR)-S0456 follows a similar physiological uptake via SMVT. Additionally, we explored whether (CR)-S0456 uptake would be altered in the presence of another small molecule vitamin that does not utilize SMVT. Folic acid cellular localization is mediated through folate receptor alpha (lung adenocarcinomas) or folate receptor beta (tumor-associated macrophages) and does not interact with SMVT. The 10–1000 \times concentration of folic acid did not alter (CR)-S0456 fluorescence in HT-1080 cells, unlike pantothenic acid and free coenzyme-R-mediated competitive inhibition (Fig. 3D, Supplementary Fig. 3, Supplementary Fig. 4). As demonstrated by the Dixon plot, there was no change in fluorescence in the presence of increasing concentrations of folic acid (Supplementary Fig. 3), indicating SMVT-specific uptake of (CR)-S0456.

Inhibiting Intracellular Metabolic, Cell Signaling, and Biotin Dependent Pathways Affects (CR)-S0456 Uptake and Cellular Localization.

To further evaluate (CR)-S0456 cellular uptake and its association with cellular proliferation, HT1080 cells were

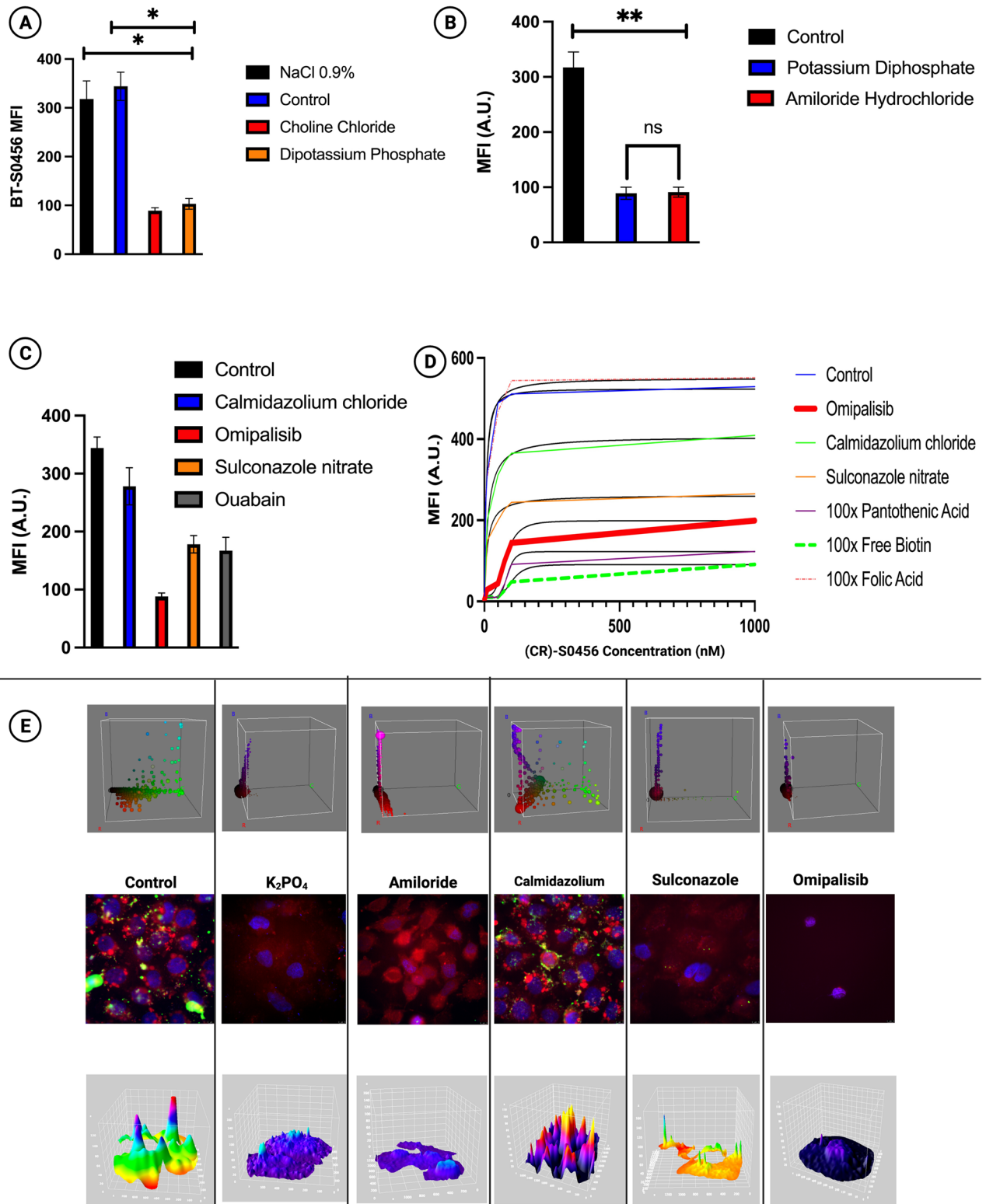


Fig. 3 **A** Replacement of Na-containing buffer with Na-free buffers (choline chloride and dipotassium phosphate) led to a significant decrease in (CR)-S0456 uptake into cells. **B** Amiloride chloride prevented (CR)-S0456 uptake into cells by blocking sodium channels. **C** Metabolic inhibitors, including calmidazolium, omipalisib, sulconazole, and ouabain, decreased (CR)-S0456 in cells, with calmidazolium producing the smallest effect. **D** Analysis of the impact of meta-

bolic inhibitors and competitive inhibition demonstrating the K_d of (CR)-S0456 in HT-1080 cells with omipalisib, pantothenic acid, and free biotin causing a marked decrease in uptake into cells. **E** ×100 objective analysis of (CR)-S0456 uptake into HT-1080 cells under various inhibitors with pixel-by-pixel color analysis (top) and surface plot analysis for (CR)-S0456 fluorescence detection (bottom) (DAPI blue, LysoTracker red, and (CR)-S0456 green).

treated with either sulconazole (holocarboxylase synthetase inhibitor), omipalisib (dual PI3K/mTOR inhibitor), or calmidazolium chloride (calmodulin inhibitor) and assessed for fluorochrome uptake.

Calmidazolium, a calmodulin inhibitor that inhibits calmodulin-dependent intracellular phosphodiesterase, has previously been found to affect coenzyme-R metabolism and cellular uptake in nutritional studies, but our analysis produced the lowest MFI change vs control, compared to other molecules (277 ± 32 vs 344 ± 19 , $p=0.09$). The effect of calmidazolium on coenzyme-R/biotin hemostasis is not clear but has been consistently reported in early physiological studies assessing the role of coenzyme-R in cellular hemostasis (Fig. 1).

Sulconazole nitrate is an imidazole-based anti-fungal that has recently been demonstrated to inhibit the holocarboxylase synthetase enzyme, which plays a critical role in activating carboxylases needed for metabolic activity (Fig. 1). These pathways have been upregulated in various malignancies, and HLCS require coenzyme-R as a cofactor. Sulconazole treatment demonstrated a nearly $2.12 \times$ change at an MFI of 155 ± 15 without affecting cellular viability ($> 92\%$ viable cells), alluding to a potential intracellular increase in coenzyme-R leading to decreased (CR)-S0456 uptake.

Omipalisib is a potent dual PI3K/mTOR inhibitor. The treatment results in the inhibition of the PI3K/Akt/mTOR pathway, leading to decreased cellular proliferation, replication, and tumorigenicity. Omipalisib treatment of HT-1080 cells demonstrated the lowest (CR)-S0456 MFI at 88 ± 6 ($p < 0.05$) (Fig. 3C, E), indicating a key requirement for coenzyme-R in the cellular proliferation of cancer cells. Given this observation, cells treated with omipalisib were used as the negative control for coenzyme-R localization.

In summary, the presence of sodium ions is critical for the cotransport of (CR)-S0456 through SMVT, in keeping with physiological coenzyme-R absorption mechanisms. Additionally, inhibition of cellular proliferation with intracellular inhibitors decreases (CR)-S0456 uptake.

(CR)-S0456 Timing and *In Vitro* Dosing Kinetics

Given the observation that (CR)-S0456 uptake correlates with the proliferative potential of cancer cells, we explored the pharmacokinetic properties of the fluorochrome to determine the optimal time and dosing *in vitro*. Renca, HT-1080, 4T1, and A549 cells demonstrated (CR)-S0456 uptake at 2 h with an MFI of 544 ± 39 . HT-1080 cells (highest average MFI) were then treated with different concentrations of (CR)-S0456 (Fig. 4C). Dosing at $10 \mu\text{M}$ produced an SBR of 287 ± 31 , whereas doses of 20 and $50 \mu\text{M}$ produced an SBR of > 400 (Fig. 6). However, nuclear staining and differentiation of cellular components via fluorescence microscopy were not evident at this supratherapeutic dose, raising

concern about cellular viability at this dose. Therefore, $10 \mu\text{M}$ was selected as the optimal dose to be used. Time analysis of (CR)-S0456 uptake demonstrated the highest SBR of 811 ± 67 at 24 h, but cellular internalization was evident at only 2 h post-incubation with the fluorochrome.

Analysis of (CR)-S0456 specificity demonstrated that $100 \times$ concentration of free unconjugated coenzyme-R caused complete inhibition of (CR)-S0456 into HT1080 cells (Fig. 4). This finding demonstrates the substrate specificity of coenzyme-R and BT-10456 toward SMVT receptors on the cell surface.

Omipalisib Activity Affects (CR)-S0456 Internalization

Given that omipalisib produced the highest decrease in (CR)-S0456 cellular localization, we explored whether this change is produced through changes in SMVT expression. SMVT expression was analyzed in wild-type HT-1080 and HEK293T cells with SDS page western blotting, demonstrating the expression of SMVT in both cell lines (Fig. 5A). When both cell lines were treated with 10 nM omipalisib, there was a decrease in the pAKT/total AKT and pmTOR/total mTOR ratios. Cell viability was also affected, with a 1.88-fold decrease in the DAPI nuclear count on fluorescence microscopy (Fig. 5E, F). The MTT assay demonstrated a 2.32-fold decrease in MTT absorbance. This correlated with relative SMVT expression on the SDS page western blot protein analysis (Fig. 5B–H). It appears that omipalisib inhibition of the AKT/mTOR pathway decreases cell proliferation with a concurrent decrease in SMVT expression, therefore limiting (CR)-S0456 absorbance. This corresponds with a $> 1000 \times$ decrease in Kd of (CR)-S0456 from baseline $8.14 \mu\text{mol}$ to 13.65 mmol . The cells in the analysis were viable with 4% trypan blue staining, demonstrating $> 95\%$ viability and a lack of (CR)-S0456 uptake. Cells that are not viable lose membrane integrity and demonstrate uniform (CR)-S0456 uptake, similar to the $50 \mu\text{M}$ dosing in Fig. 5C.

Biodistribution Assessment of (CR)-S0456 in Small Animal Models Demonstrates No Uptake in Lung Parenchyma

Due to the specificity of (CR)-S0456 to SMVT and its correlation with coenzyme-R cellular uptake homeostasis, as well as the ubiquitous need for coenzyme-R in normal cellular metabolism, we evaluated the biodistribution of (CR)-S0456 in athymic nude mice bearing flank xenografts to recognize the ideal solid organ amenable for (CR)-S0456-guided cancer resection (Fig. 6). Immunocompromised mice were injected with different concentrations of (CR)-S0456 at 0 mg/kg , 1 mg/kg (0.77 mM), 1.41 mM (2 mg/kg), or 3.42 mM (5 mg/kg) and imaged at various time points. As

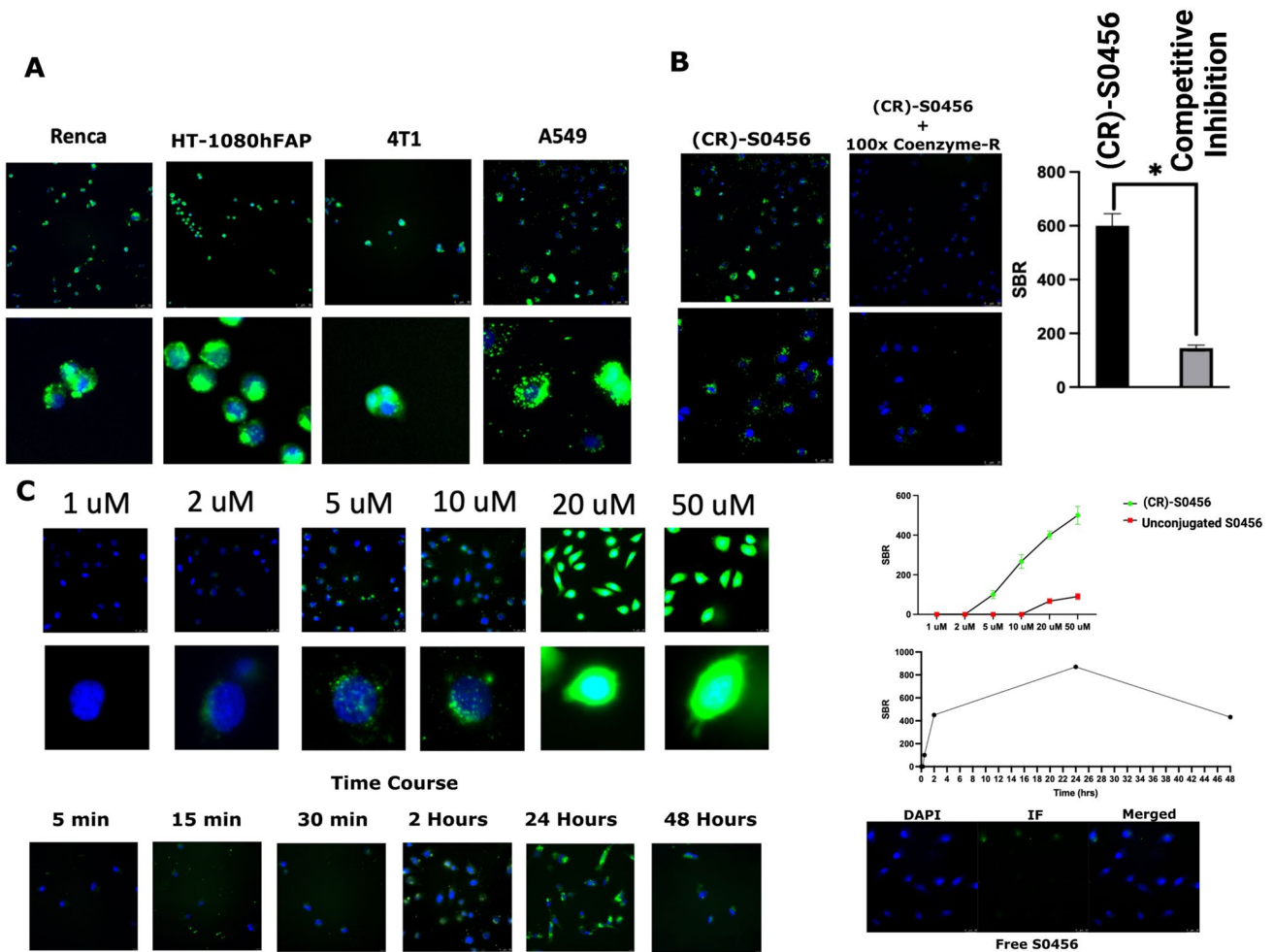


Fig. 4 **A** (CR)-S0456 uptake into metabolically active cells. **B** (CR)-S0456 uptake is competitively inhibited with free coenzyme-R coadministration. **C** Dosing and biodistribution studies demonstrate (CR)-S0456 fluorescence emission with various doses and time courses.

seen in Fig. 7, several gastrointestinal visceral organs had an uptake of (CR)-S0456, including the liver (6.43 ± 0.32), colon (5.11 ± 0.39), small intestine (2.91 ± 0.44), kidneys (8.21 ± 0.49), and stomach (3.11 ± 0.34) ($p = 0.23$), measured at 24 h. There was no uptake of (CR)-S0456 in the lungs, heart, pancreas, or brain. When mice had HT-1080 xenografts established, 2 and 5 mg/kg produced the highest TBR (3.89 ± 0.26 vs 4.08 ± 0.31 , respectively) at 24 h. Therefore, the lowest 2 mg/kg was selected for the study. The highest TBR was also observed at 24 h postinjection (Fig. 6).

Ompalisib Treatment Suppresses HT-1080 (CR)-S0456 Uptake

Given the observed (CR)-S0456 cellular uptake changes with ompalisib treatment *in vivo*, we explored whether similar observations would be evident in small animal models. HT-1080 xenografts with a minimum tumor volume of 500

mm³ were injected intraperitoneally with 10 nM ompalisib biweekly for 28 days. At the end of the time frame, the mice were injected with 2 mg/kg (CR)-S0456 24 h prior to imaging. Tumors treated with ompalisib had no uptake of (CR)-S0456 compared to the untreated group (Fig. 7). The change in (CR)-S0456 was most evident in treated tumors without any changes noted in visceral biodistribution compared to the baseline and untreated groups ($p < 0.05$). On histologic assessment and fluorescence microscopy, treated tumors did not demonstrate (CR)-S0456 localization. Protein lysates of xenografts demonstrated decreased expression of mTOR and pAKT and decreased relative expression of SMVT (Figs. 7 and 8).

Analysis of SMVT expression in cells and tumors treated with ompalisib demonstrated a significant decrease in HT1080 cell SMVT staining by IHC. This correlated with (CR)-S0456 uptake both *in vitro* and *in vivo* (Fig. 8A). To further visualize cytologic distribution patterns of the coenzyme-R conjugate, we analyzed intratumoral fluorescence using NIR needle confocal laser endomicroscopy

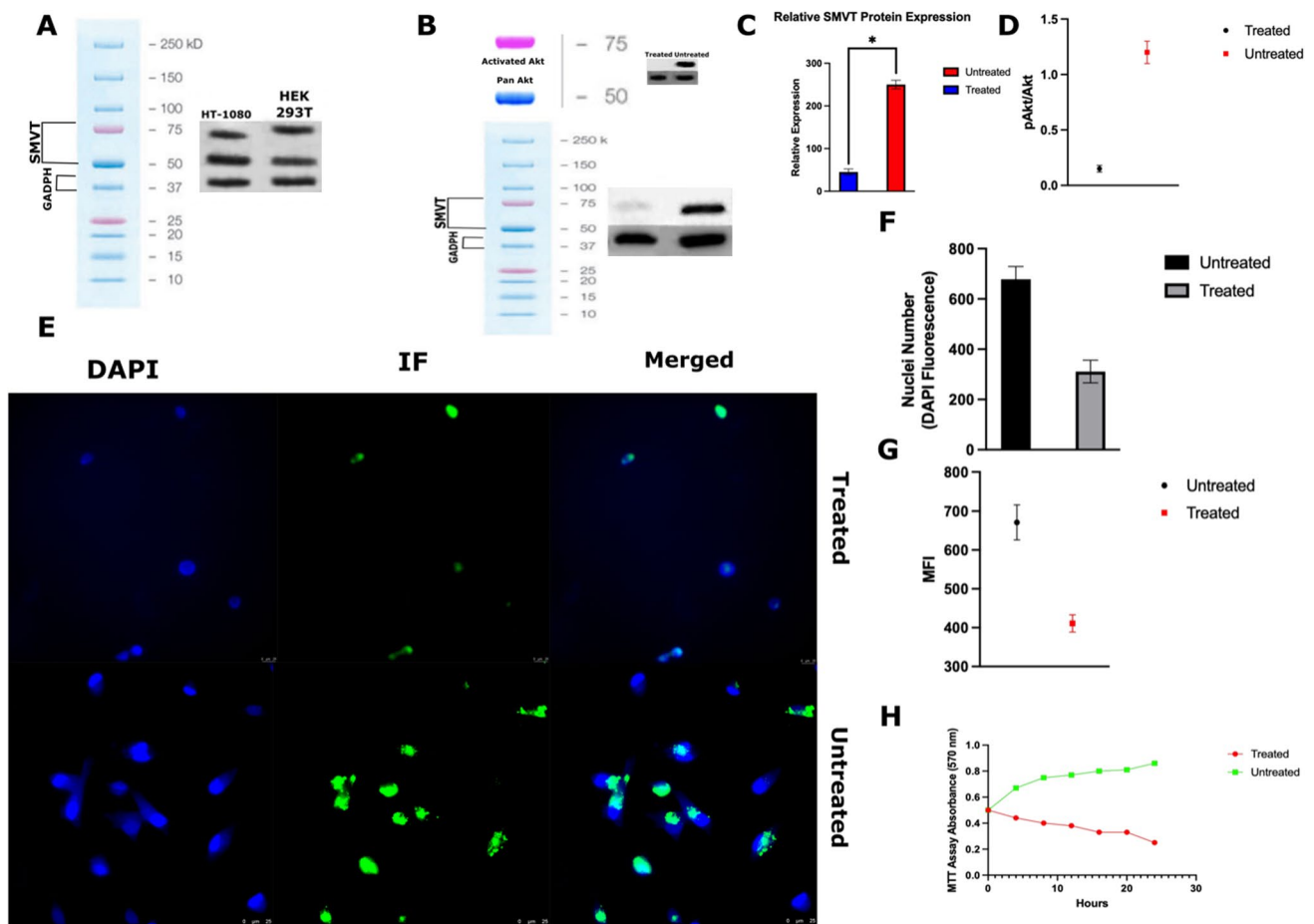


Fig. 5 **A** Both HT-1080 and HEK293T cells express SMVT, as evidenced by the uptake of biotin in both cell lines, with HT-1080 demonstrating higher uptake. **B** Omipalisib inhibits PI3K/mTOR activity in HT-1080 cells with corresponding decreased expression in **C** SMVT and pAKT/AKT ratio **D** in the treated group. **E** Omipalisib inhibits (CR)-S0456 uptake into treated HT-1080 cells with a cor-

responding decrease in nuclei count in these cells. **F, G** Treatment inhibits fluorescence via (CR)-S0456 and the proliferative potential of cells, leading to a decrease in SMVT cellular expression. This translates to decreased uptake of (CR)-S0456 by viable HT-1080 cells. **H** as demonstrated decrease in MTT assay of the treated cells correlating with decrease in fluorophore uptake.

(NIR nCLE) (Fig. 8C, Video 1). Live hFAP + HT1080 xenograft-bearing mice (both the wild-type and omipalisib cohorts) were infused with either 2 mg/kg (CR)-S0456 or FAPL-S0456. FAPL-S0456 has similar fluorescence parameters as (CR)-S0456 since the fluorescent fluorochrome (S0456) is the same for both molecules but is targeted to the fibroblast activation protein transmembrane receptor instead of SMVT. Live xenograft imaging using nCLE demonstrated (CR)-S0456 fluorescence and FAPL-S0456 fluorescence in the untreated wild-type group (Fig. 8C). Conversely, the omipalisib-treated group, concordant with the IHC findings, demonstrated a lack of (CR)-S0456 fluorescence. Mice treated with omipalisib but infused with FAPL-S0456 demonstrated strong fluorescence emission detection by nCLE (Fig. 8C, Video 1). These results suggest that targeting intracellular proliferative pathways such as PI3K/AKT signaling inhibits coenzyme-R uptake and intracellular biotinylation.

Discussion

The utilization of IMI over the last decade has been exponentially increasing and is now becoming a common intraoperative tool for surgical oncologists [4, 15–17]. The natural synergy of IMI with minimally invasive techniques has allowed real-time rapid assessment of primary lesion resection, assessment of oncologic margins, and detection of occult nonpalpable lesions [18]. However, given the existing heterogeneity among tumors and the surrounding microenvironment, not all patients benefit from the technology, as their tumors might not express the receptors necessary for targeted fluorochromes. Therefore, there remains a need to develop a novel fluorochrome that can target a wide variety of tumors across all patient groups. In this study, we explored coenzyme-R conjugated NIR fluorochrome (S0456) as a potential solution for labeling various metabolically active tumors. We demonstrated that (CR)-S0456

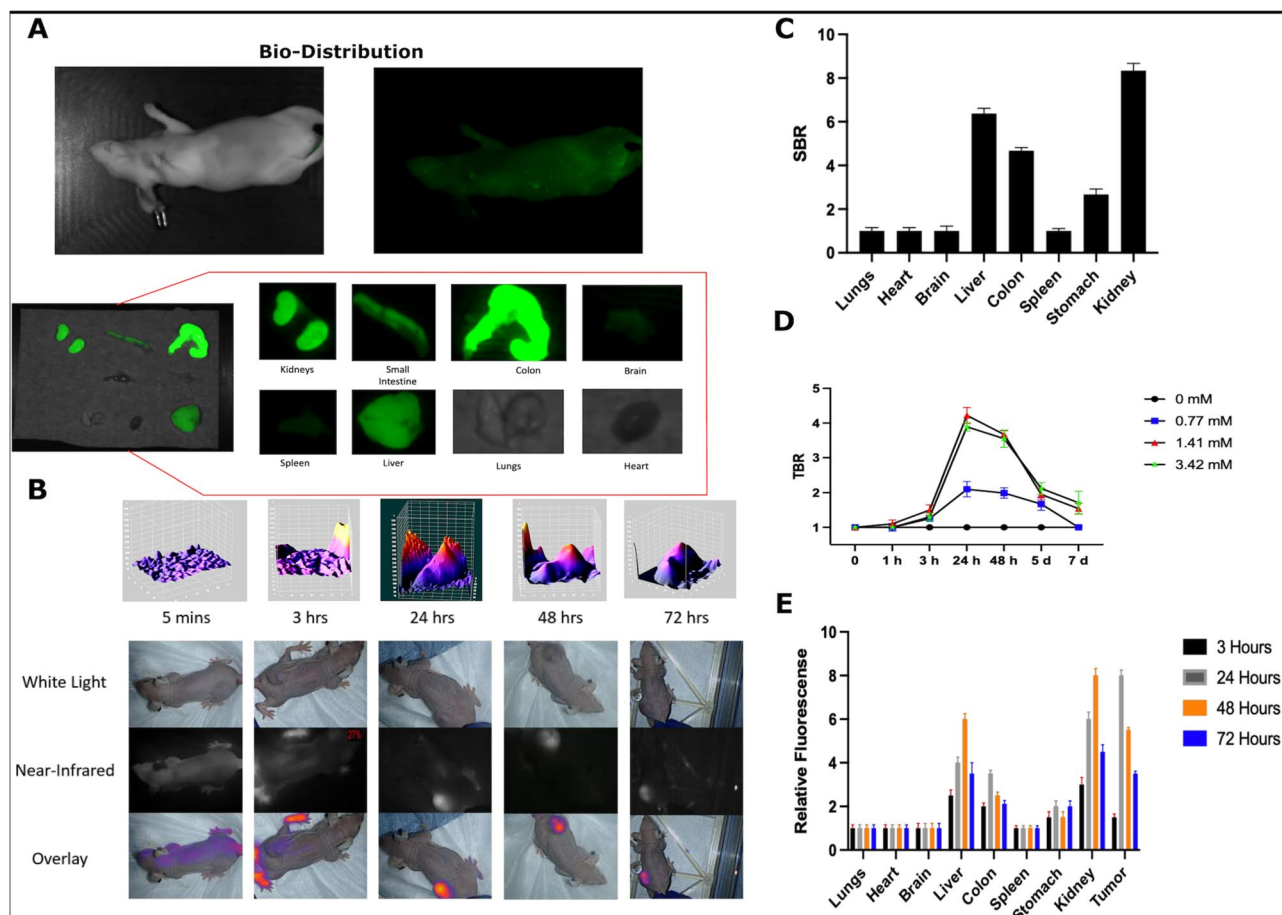


Fig. 6 **A** Biodistribution of (CR)-S0456 in athymic nude mice administered 5 mg/kg 24 h prior demonstrating expected (CR)-S0456 fluorescence in the gastrointestinal tract, liver, and kidneys (known excretion of S0456). **B** Twenty-four hours postinjection produced the

highest tumor fluorescence in HT-1080-bearing xenografts. **C–E** The timing and biodistribution of (CR)-S0456 with the highest concentration noted in the tumor at 24 h.

localizes intracellularly through the small molecule vitamin transporter and that its localization can be disrupted by inhibiting cellular proliferation via PI3K/mTOR inhibition, seizing intracellular biotinylation via HLCS inhibition, and competitive inhibition.

Coenzyme-R (vitamin B₇) is an essential substrate for all eukaryotic cells (Fig. 1) [8, 19]. In humans, it is not synthesized naturally and must be supplemented exogenously. The molecule plays an essential role in various metabolic pathways by being a key activating cofactor of various carboxylases and playing a key role in epigenetic activation via histone modification (Fig. 1) [10]. Not surprisingly, highly metabolically active cancer cells have hijacked coenzyme-R uptake mechanisms to support the cellular metabolism needed for tumorigenicity (Supplementary Fig. 1) [20]. Previous literature reports have highlighted increased intracellular biotin expression in various tumors, which has also correlated with aggressiveness and poor outcomes. Similarly, we noticed significant mutations and SLC5A6 mutations

across various tumor types when looking at TCGA analysis (Supplementary Fig. 1) [21]. Furthermore, in our various cell lines, (CR)-S0456 fluorescence intensity linearly correlated with proliferative potential. Cells with lower doubling time, high MTT absorbance, and higher colony-forming units had significantly higher (CR)-S0456 fluorescence than HEK293T and B16 cells (Fig. 2). This is in agreement with literature reports of the ubiquitous and essential nature of coenzyme-R, as all cells will require differing levels of coenzyme-R, but those that are proliferating at a high rate will need to consume more, leading to higher intracellular concentration and fluorescence intensity [10, 22, 23].

Given that there was an observed significant difference in (CR)-S0456 localization based on cellular proliferation, we wanted to explore whether inhibiting various pathways where biotinylation plays a key role will inhibit (CR)-S0456 localization (Fig. 1). Extensive initial evaluation of coenzyme-R homeostasis has demonstrated that SMVT, which is a Na⁺ cotransporter of coenzyme-R

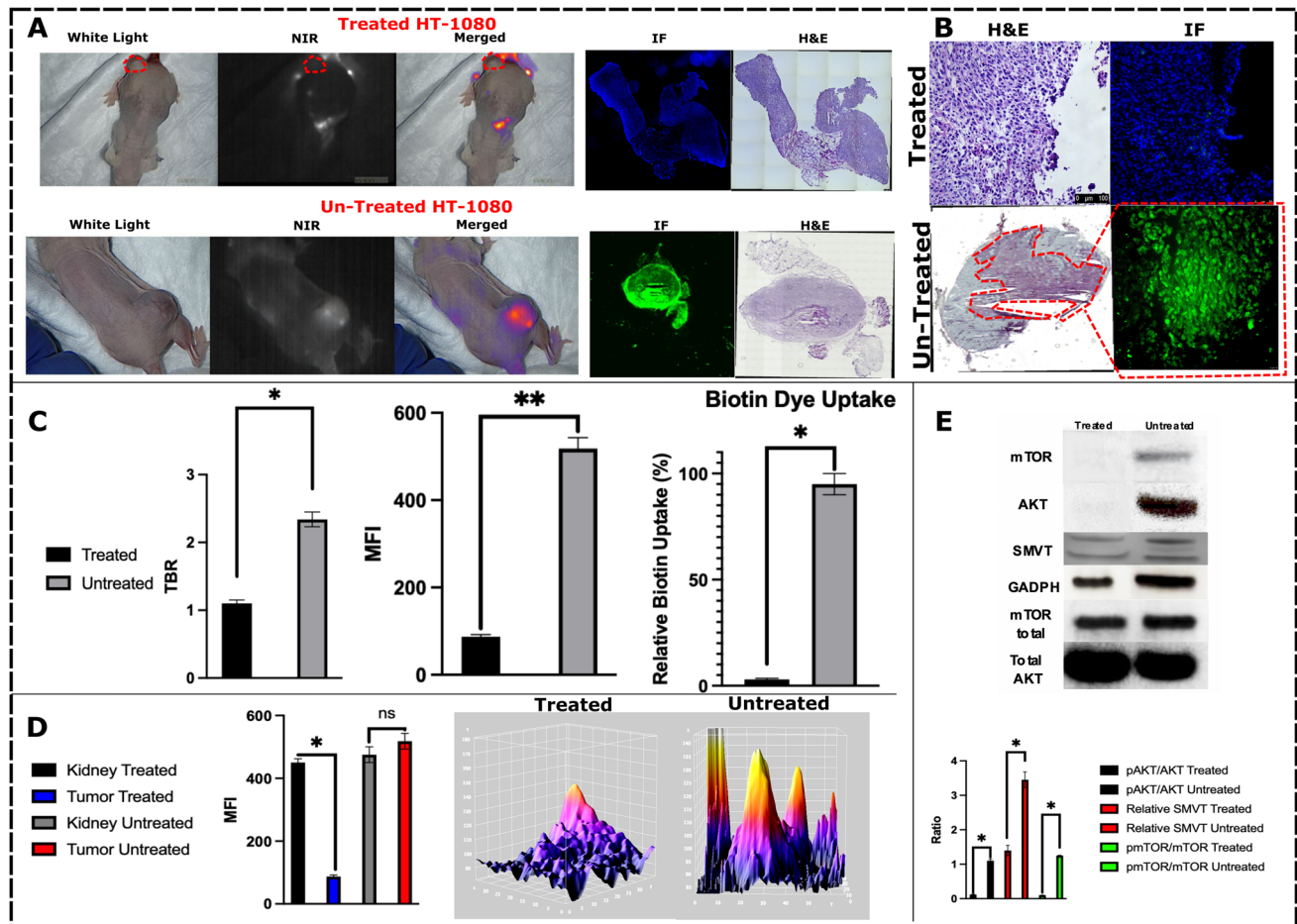


Fig. 7 **A** Xenografts treated with omipalisib (treated) had no tumor fluorescence uptake compared to HT-1080 cells that did not undergo any treatment (untreated). **B** This translated to fluorescence microscopic analysis demonstrating no intratumoral and intracellular fluorochrome uptake in the treatment group. **C** Fluorescence emission analysis of the two treatment groups demonstrated decreased TBR, tumor MFI, and biotin uptake in the treatment group. **D** There was no

change in renal fluorescence, which is a known excretion of S0456, in either group, while there was a considerable decrease in the omipalisib group, demonstrating that the tracer was distributed intravenously but did not localize to tumors. **E** Treatment group had expected a decrease in AKT/mTOR pathway with a decrease in SMVT expression in densitometric analysis.

and pantothenic acid, is a major transporter involved in vitamin uptake [24]. Removing Na ions from the buffers by substituting chloride or potassium ions demonstrated minimal to no uptake of (CR)-S0456 (Fig. 3). When the same cells that were initially incubated with Na⁺-free buffers were then reintroduced to normal Na⁺-containing buffer solutions, they demonstrated (CR)-S0456 uptake similar to that of control cells. This is in line with previous tagged coenzyme-R studies [24, 25, 25]. Furthermore, to demonstrate the Na⁺ ion requirement for (CR)-S0456 uptake, we pretreated the cells with amiloride (Na⁺ channel blocker), which prevented (CR)-S0456 cell labeling similar to removing Na⁺ from buffers (Fig. 3). These findings demonstrate that (CR)-S0456 uptake follows known physiological vitamin intracellular uptake and specifically through the Na cotransporter (Fig. 3).

Although we demonstrated (CR)-S0456 receptor specificity, we wanted to explore whether manipulating cellular proliferation would disturb (CR)-S0456 uptake into cells. Fibrosarcoma (HT1080) cell lines were treated with various metabolic inhibitors, such as calmidazolium chloride, omipalisib, ouabain, and sulconazole nitrate. Sulconazole has recently been demonstrated to inhibit HLCS, which requires biotinylation as a key step [10]. The inhibition of HLCS will theoretically inhibit other carboxylases that control various points of cellular metabolism, including cholesterol synthesis, glucose metabolism, and lipid metabolism (Fig. 1). Calmidazolium caused the lowest (CR)-S0456 change compared to baseline, but the difference observed in fluorescence intensity was not statistically significant. Omipalisib, on the other hand, produced the highest decrease in (CR)-S0456 uptake. Sulconazole

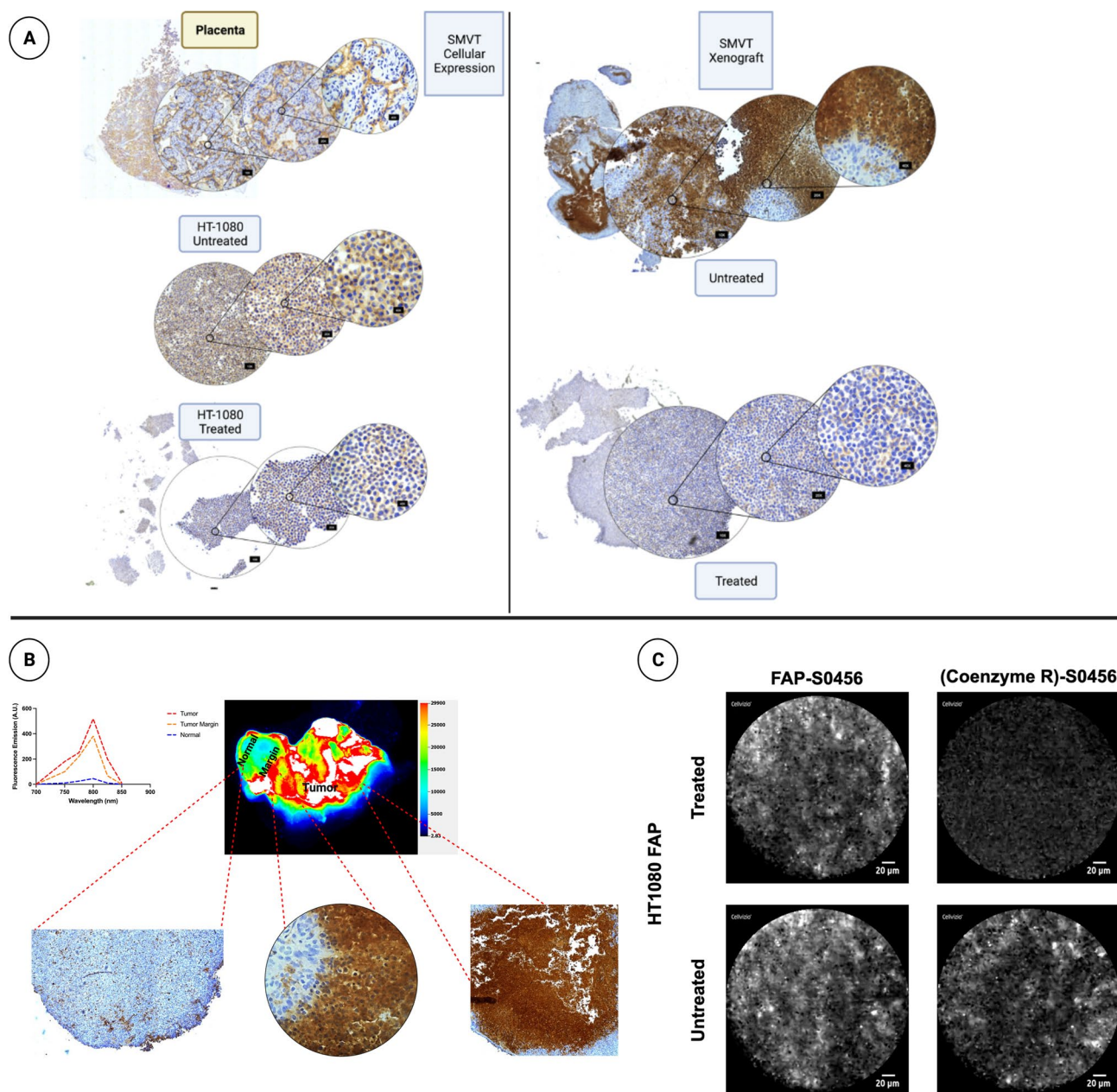


Fig. 8 **A** IHC analysis of mouse tumors demonstrates a lack of SMVT expression in cells (left) treated with omipalisib. The results correlated with HT-1080 xenograft IHC (right) in mice undergoing omipalisib injection. Placental tissue, known for the highly consistent expression of SMVT, was used as a staining control. **B** (CR)-S0456 can identify primary tumor nodules, tumor margins, and normal parenchyma using NIR imaging, which is concordant with histopathological analysis. **C** NIR-nCLE intratumoral assessment of the

hFAP-transfected HT-1080 xenografts treated with omipalisib demonstrated the absence of (CR)-S0456 uptake and fluorescence emission. Omipalisib-treated hFAP+ xenografts demonstrated fluorescence of the FAP ligand S0456 conjugate, indicating the viability of tumor cells and a specific decrease in the uptake of the biotin conjugate. Conversely, untreated hFAP+ HT1080 xenografts demonstrated both the presence of (CR)-S0456 and FAPL-S0456 fluorescence with nCLE. Full sequences are demonstrated in Video 1.

and ouabain did not completely inhibit (CR)-S0456 uptake but caused a 2.12-fold decrease in fluorescence in the cells ($p < 0.05$). These results further suggest that coenzyme-R is an essential vitamin that is needed in various physiological cellular processes and that altering the metabolic and proliferative potential of cells via various therapeutic

agents will produce changes in coenzyme-R homeostasis within them (Fig. 3).

To further understand how omipalisib decreased (CR)-S0456 uptake in viable cells, we examined the cellular expression of SMVT. The cells treated with omipalisib demonstrated both mTOR and Akt pathway inhibition but,

interestingly, also demonstrated a significant decrease in SMVT protein expression (Fig. 5). On immunohistochemical analysis, treated cells had minimal to no SMVT staining compared to 3+ staining noted in wild-type untreated cells (Fig. 8). The SMVT expression change correlated with (CR)-S0456 uptake and cellular fluorescence. Previous literature reports have observed similar findings, further indicating the substrate specificity of (CR)-S0456 through SMVT transport channels [5, 24, 26].

One of the concerns with using a ubiquitous small molecule vitamin is the potential localization to normal parenchyma, leading to an increase in background fluorescence that would limit tumor-to-background contrast differentiation. Biodistribution in ATHYMIC NUDE mice demonstrated excellent HT1080 xenograft localization and labeling with (CR)-S0456 (Fig. 6). However, when analyzing the biodistribution of (CR)-S0456, several organs, including the colon, small intestine, liver, and kidney, demonstrated fluorescence. This is not surprising, as this is consistent with known coenzyme-R uptake, as it is acquired through diet and processed in the liver. However, the lung and brain had low to no (CR)-S0456 fluorescence under normal conditions, making them the ideal organ systems to explore during IMI-guided resections (Figs. 6 and 7). Pulmonary metastasis from colorectal and hepatocellular malignancies is considerable, and (CR)-S0456 could be a suitable NIR fluorochrome to explore for these tumors [27].

In vitro (CR)-S0456 was significantly decreased with omipalisib administration, which correlated with SMVT expression. We wanted to explore whether this would be applicable to xenograft models as well. HT1080 cells treated with omipalisib demonstrated no uptake of (CR)-S0456 compared to untreated HT-1080 cells (Figs. 7 and 8). Tumor lysates demonstrated suppression of the AKT/mTOR pathway as well as significantly decreased expression of SMVT. Further analysis for SMVT via IHC demonstrated 3+ transporter staining in wild-type untreated cells, whereas omipalisib treatment led to a near-complete absence of SMVT in HT1080 tumors (Figs. 7 and 8). It appears that when cell proliferation is inhibited, SMVT expression is downregulated to control the intracellular coenzyme-R concentration and further expressed during proliferative phases. Our analysis of intratumoral single-cell fluorescence using novel NIR-nCLE-guided imaging similarly demonstrated a lack of biotin uptake into HT-1080 cells, but the treated cells demonstrated FAP-targeted S0456 fluorescence. This demonstrates that the targeting of the proliferative pathways causes metabolic downregulation and essential vitamin uptake, which can be exploited in cancer imaging as well as treatment (Fig. 8C, Video 1). We believe that (CR)-S0456 can be used to exploit this phenomenon in aggressive fibrosarcomas, particularly when considering that 30–50% of patients with aggressive sarcomas develop pulmonary

metastases. Pulmonary metastasectomy in this population offers a survival advantage and represents an important future avenue to be explored [27, 28].

There are several limitations that need to be acknowledged during this study. A significant portion of the (CR)-S0456 evaluation and biotin homeostasis was performed *in vitro* and in mouse models. These preclinical models only crudely estimate the tumor microenvironment in humans. This is an important consideration, particularly with abundant vitamins, such as biotin, which can lead to false positive fluorescence from cancer-associated fibroblasts or resident macrophages in the extracellular matrix. While the absence of (CR)-S0456 in the lungs is encouraging as a potential avenue to explore fluorochrome utilization for NIR IMI-guided resections, further studies in large animals will be needed to delineate this. Additionally, in the era of personalized medicine and tumor characterization for immune checkpoint inhibitor therapies, a significant number of patients undergo neoadjuvant therapies. Certainly, in appropriate patient populations, this leads to substantial radiologic and pathologic resolution of certain tumors. We foresee this neoadjuvant treatment population posing a challenge for coenzyme-R guided resections as these tumors would demonstrate metabolic and transcriptional halting that can lead to a lack of fluorescence and non-localization as evident in our preclinical models. This should be astutely recognized in future clinical trials.

Conclusion

In conclusion, Coenzyme-R conjugated NIR fluorochrome follows physiological coenzyme-R intracellular localization through the small molecular vitamin transporter that is overexpressed in aggressive malignant cells. Treatment with chemotherapeutic regimens alters metabolic machinery and leads to decreased SMVT expression and (CR)-S0456 uptake. Additionally, (CR)-S0456 localizes to xenografts and demonstrates high NIR fluorescence emission compared to normal visceral parenchyma. Our analysis demonstrates the high affinity and specificity of (CR)-S0456 for SMVT-expressing tumors and its excellent safety profile, making (CR)-S0456 a suitable NIR tracer conjugate in IMI-guided lung cancer or pulmonary metastases, as there is no background uptake in the lung. Further preclinical studies are needed to confirm its safety and efficacy, but the results indicate the potential promise of (CR)-S0456 in the management of patients with primary and metastatic sarcomas and colorectal malignancies.

Abbreviations IMI: Intraoperative molecular imaging; CR: Coenzyme R; SMVT: Sodium dependent multivitamin transporter; NIR: Near infrared; HLCS: Holocarboxylase synthetase

Supplementary Information The online version contains supplementary material available at <https://doi.org/10.1007/s11307-022-01792-4>.

Acknowledgements We would like to thank Drs. Steven Albelda and Philip Low for material and cell line support.

Author Contribution FA, GTK, JD, and SS: study design, data validation, manuscript draft, manuscript finalization, and review. AC, NTS, AS, EB, BA, and EE: data acquisition and experiment conduction.

Funding Dr. Azari was supported by the training grant in surgical oncology from the National Institutes of Health (T32CA251063-01), the Society of Thoracic Surgeons Thoracic Surgery Foundation Research Award, and the Stephen C. Cheung Award in Surgical Oncology. Dr. Singhal was supported by the National Institutes of Health (R01 CA193556) and the State of Pennsylvania Health Research Formula Fund. Dr. Kennedy was supported by the American Philosophical Society and the National Institutes of Health (F32 CA254210-01). Dr. Sullivan was supported by NIH T32 postdoctoral fellowship (NIH T32 CA009140).

Data Availability The data generated in this study are displayed in the manuscript and supplemental files. Data is available upon request from the corresponding author.

Material Availability The data generated in this study are displayed in the manuscript and supplemental files. Data is available upon request from the corresponding author.

Declarations

Ethics Approval and Consent to Participate All experiments have been approved by the University of Pennsylvania Institutional Review Board. Animal studies were performed according to protocols approved by the University of Pennsylvania Institutional Animal Care and Use Committee (IACUC) in accordance with the National Institutes of Health guidelines.

Consent for Publication N/A

Competing Interests S.S. has been named a co-inventor and submitted a patent to the USPTO regarding the fluorochrome. In order to protect intellectual property while the patent application process is pending, the structure is omitted from the manuscript. The structure is readily available by contacting the corresponding author and the University of Pennsylvania Intellectual Protection Office.

References

- Fedor D, Johnson WR, Singhal S (2013) Local recurrence following lung cancer surgery: incidence, risk factors, and outcomes. *Surg Oncol* 22:156–161
- Azari F et al (2022) State of the art: precision surgery guided by intraoperative molecular imaging. *J Nucl Med*. <https://doi.org/10.2967/jnumed.121.263409>
- Chi C et al (2014) Intraoperative imaging-guided cancer surgery: from current fluorescence molecular imaging methods to future multi-modality imaging technology. *Theranostics* 4:1072–1084
- Azari F et al (2021) Intraoperative molecular imaging clinical trials: a review of 2020 conference proceedings. *JBO* 26:050901
- Sukjoi W et al (2020) Overexpression of holocarboxylase synthetase predicts lymph node metastasis and unfavorable prognosis in breast cancer. *Anticancer Res* 40:4557–4565
- Scheerger SB, Zempleni J (2003) Expression of oncogenes depends on biotin in human small cell lung cancer cells NCI-H69. *Int J Vitam Nutr Res* 73:461–467
- Kiesel VA et al (2021) Pyruvate carboxylase and cancer progression. *Cancer Metab* 9:20
- Zempleni J, Liu D, Camara DT, Cordonier EL (2014) Novel roles of holocarboxylase synthetase in gene regulation and intermediary metabolism. *Nutr Rev* 72:369–376
- Solórzano-Vargas RS, Pacheco-Alvarez D, León-Del-Río A (2002) Holocarboxylase synthetase is an obligate participant in biotin-mediated regulation of its own expression and of biotin-dependent carboxylases mRNA levels in human cells. *Proc Natl Acad Sci* 99:5325–5330
- Yoon J et al (2021) A chemical biology approach reveals a dependency of glioblastoma on biotin distribution. *Sci Adv* 7:eabf6033
- Vadlapudi AD, Vadlapatla RK, Mitra AK (2012) Sodium dependent multivitamin transporter (SMVT): a potential target for drug delivery. *Curr Drug Targets* 13:994–1003
- Patel M, Vadlapatla RK, Shah S, Mitra AK (2012) Molecular expression and functional activity of sodium dependent multivitamin transporter in human prostate cancer cells. *Int J Pharm* 436:324–331
- Fam KT, Collot M, Klymchenko AS (2020) Probing biotin receptors in cancer cells with rationally designed fluorogenic squaraine dimers. *Chem Sci* 11:8240–8248
- Cerami E et al (2012) The cBio Cancer Genomics Portal: an open platform for exploring multidimensional cancer genomics data. *Cancer Discov* 2:401–404
- Hadjipanayis CG, Widhalm G, Stummer W (2015) What is the surgical benefit of utilizing 5-ALA for fluorescence-guided surgery of malignant gliomas? *Neurosurg* 77:663–673
- Lee SJ, Choi YY, Kim C, Chung MS (2017) Correlations between tumor to background ratio on breast-specific gamma imaging and prognostic factors in breast cancer. *J Korean Med Sci* 32:1031–1037
- Lee JY-K et al (2016) Intraoperative near-infrared optical imaging can localize gadolinium-enhancing gliomas during surgery. *Neurosurg* 79:856–871
- Azari F, Kennedy G, Singhal S (2020) Intraoperative detection and assessment of lung nodules. *Surg Oncol Clin* 29:525–541
- Pinon V, Ravel S, Douce R, Alban C (2005) Biotin synthesis in plants. The first committed step of the pathway is catalyzed by a cytosolic 7-keto-8-aminopelargonic acid synthase. *Plant Physiol* 139:1666–1676
- Song X et al (2021) Construction of a biotin-targeting drug delivery system and its near-infrared theranostic fluorescent probe for real-time image-guided therapy of lung cancer. *Chin Chem Lett*. <https://doi.org/10.1016/j.ccllet.2021.08.111>
- Sun T et al (2020) Integrated profiling identifies SLC5A6 and MFAP2 as novel diagnostic and prognostic biomarkers in gastric cancer patients. *Int J Oncol* 56:460–469
- Hassan YI, Zempleni J (2006) Epigenetic regulation of chromatin structure and gene function by biotin. *J Nutr* 136:1763–1765
- Park S, Kim E, Kim WY, Kang C, Kim JS (2015) Biotin-guided anticancer drug delivery with acidity-triggered drug release. *Chem Commun* 51:9343–9345

24. Vadlapudi AD, Vadlapatla RK, Pal D, Mitra AK (2013) Biotin uptake by T47D breast cancer cells: functional and molecular evidence of sodium-dependent multivitamin transporter (SMVT). *Int J Pharm* 441:535–543
25. Said HM et al (1998) Biotin uptake by human colonic epithelial NCM460 cells: a carrier-mediated process shared with pantothenic acid. *Am J Physiol Cell Physiol* 275:C1365–C1371
26. Stanley JS, Griffin JB, Zempleni J (2001) Biotinylation of histones in human cells. *Eur J Biochem* 268:5424–5429
27. Treasure T, Fiorentino F, Scarci M, Møller H, Utley M (2012) Pulmonary metastasectomy for sarcoma: a systematic review of reported outcomes in the context of Thames Cancer Registry data. *BMJ Open* 2(5):e001736. <https://doi.org/10.1136/bmjopen-2012-001736>
28. Digesu CS, Wiesel O, Vaporciyan AA, Colson YL (2016) Management of sarcoma metastases to the lung. *Surg Oncol Clin N Am* 25:721–733

Publisher's Note Springer Nature remains neutral with regard to jurisdictional claims in published maps and institutional affiliations.

Springer Nature or its licensor (e.g. a society or other partner) holds exclusive rights to this article under a publishing agreement with the author(s) or other rightsholder(s); author self-archiving of the accepted manuscript version of this article is solely governed by the terms of such publishing agreement and applicable law.

Authors and Affiliations

Feredun Azari^{1,2,3}  · Gregory T. Kennedy^{1,2} · Ashley Chang^{1,2} · Bilal Nadeem^{1,2} · Patrick Bou-Samra^{1,2} · Austin Chang^{1,2} · Alix Segil^{1,2} · Elizabeth Bernstein^{2,4} · Neil T. Sullivan^{2,4} · Evgeniy Eruslanov^{2,4} · James Delikatny^{2,4} · Sunil Singhal^{1,2}

¹ Department of Thoracic Surgery, University of Pennsylvania Perelman School of Medicine, Philadelphia, PA, USA

² University of Pennsylvania Perelman School of Medicine, Philadelphia, PA, USA

³ Department of Thoracic Surgery, Hospital of the University of Pennsylvania, 3400 Civic Center Boulevard, 14th floor, South Pavilion, Philadelphia, PA 19104, USA

⁴ Department of Radiology, University of Pennsylvania Perelman School of Medicine, Philadelphia, PA, USA